Hannes Ernst*, Matthieu Scherpf, Hagen Malberg and Martin Schmidt

Pulse Arrival Time - A Sensitive Vital Parameter for the Detection of Mental Stress

Abstract: Mental stress triggers positive inotropic and chronotropic effects as well as peripheral vasoconstriction. This alters the pulse arrival time (PAT), the duration between electrical excitation of the ventricles and arrival of the pulse wave in the periphery. We conducted a study to examine PAT during five rest blocks and under mental stress utilizing the Mannheim Multicomponent Stress Test. Electrocardiograms as well as finger and earlobe photoplethysmograms were recorded. PAT was calculated for over 135,000 heartbeats from 42 healthy volunteers as the time duration between the R peak in the electrocardiogram and the following pulse onset in the respective photoplethysmogram. To identify the effect of mental stress, block-wise PAT means were statistically analyzed with repeated measures ANOVA. The analyses showed significant differences between the block means for both PAT measures ($p < 0.001$). Post-hoc tests revealed significantly reduced PAT during the stress block compared to all rest blocks for both PAT measures ($p < 0.001$). We found no significant differences between the rest blocks. Our results support that PAT is a sensitive vital parameter for the detection of mental stress in healthy volunteers. This holds true for both measurement positions, the finger and the earlobe.

Keywords: pulse arrival time, pulse transit time, mental stress, measurement synchronization.

https://doi.org/10.1515/cdbme-2021-2106

1 Introduction

Mental stress triggers reactions of the autonomic nervous system. Positive inotropic and chronotropic effects as well as peripheral vasoconstriction increase the blood pressure and thus the speed with which the pulse wave propagates through the vascular system [1]. This makes pulse arrival time (PAT), defined as the duration between electrical excitation of the ventricles and arrival of the pulse wave in the periphery [2], a promising candidate for the detection of mental stress [3].

In this work, we present PAT measures derived from an electrocardiogram (ECG) and photoplethysmograms (PPGs) from the left index finger and the left earlobe at rest and under mental stress.

2 Methods and Materials

The study described below is covered by permission EK 411092019 of the TU Dresden Ethics Committee, an institutional review board officially registered at the Office for Human Research Protections (IRB00001473, IORG0001076).

2.1 Setup

We conducted a study to examine PAT during rest and under mental stress. After initial questionnaires and preparation (electrode and sensor attachment), participants rested for 5 min. Participants were then introduced to the test environment by a small training session. We used the Mannheim Multicomponent Stress Test (MMST) [4], [5] to induce mental stress. The MMST combines several stressors with focus on an arithmetic task (PASAT-C) and took 4 – 5 min. To observe recovery effects, four rest blocks (1 x 5 min, 3 x 10 min) followed the MMST. During all rest blocks, participants watched a relaxation video of an idyllic beach bay and were free to close their eyes. Figure 1 summarizes the structure of the experiment.

The setup combined several measurement units, among them a Task Force® Monitor 3040i (CNSystems Medizintechnik GmbH, Graz, Austria), short TFM, and an ADInstruments PowerLab® 16/35 (ADInstruments Ltd., Dunedin, New Zealand), short ADI. From the initial rest block on, the TFM recorded a 2-channel ECG (Einthoven I and II) with a sampling frequency of 1000 Hz and the ADI recorded two PPGs at the left index finger (MLT1020FC,

***Corresponding author: Hannes Ernst:**
Research Training Group Conducive Design of Cyber-Physical Production Systems, TU Dresden, Dresden, Germany,
e-mail: hannes.ernst@tu-dresden.de
Matthieu Scherpf, Hagen Malberg, Martin Schmidt:
Institute of Biomedical Engineering, TU Dresden, Dresden, Germany

ADInstruments Ltd.) and the left earlobe (MLT1020EC, ADInstruments Ltd.) with a sampling frequency of 1000 Hz. To synchronize the two units, an analogue sync signal was generated by the PowerLab® and recorded by both units with a sampling frequency of 1000 Hz. The sync signal consisted of several predefined waveforms such as sine, sawtooth, and triangle and repeated itself every 10 minutes (see Figure 2). This setup enabled the recording of high-resolution signals with verifiable synchronization, which is the technical prerequisite for accurate PAT measurement.

1	2	3	4	5	6	block
5	8 - 10	5	10	10	10	T in min
R	MMST	R	R	R	R	state

Figure 1: Temporal structure of the experiment with block durations T. R stands for rest. MMST includes the training phase and the actual stress test. After each block, there was a break of 3 – 4 min.

2.2 Data Processing

Data processing was performed with MATLAB® 2020b (The MathWorks, Inc., Natick MA, USA) and consisted of five steps: 1) signal synchronization, 2) signal filtering, 3) signal annotation, 4) annotation validation, and 5) PAT calculation.

Signal synchronization: At first, the two initial signal edges of the sync signals were superimposed. We noticed that the two sync signals diverged over time as the real sampling frequencies of ADI and TFM differed slightly. To compensate this effect, we time-stretched the TFM signals (see Figure 2). We tested time-stretching factors representing sample rates from 997 – 1000 Hz with a step size of 0.01 Hz. Both, the time-stretched TFM sync signal and the ADI sync signal were z-scored and linearly resampled to the same time vector with 10 kHz resolution. Between these two signals, the absolute difference was calculated. The optimal time-stretching factor was identified by the minimum absolute difference. The determined time-stretching factor was then applied to the ECG.

Signal filtering: The ECG channel Einthoven II was used and filtered with a 5th order butterworth bandpass with cutoff frequencies 0.5 Hz and 25 Hz. The PPGs were also filtered with a 5th order butterworth bandpass, but with cutoff frequencies 0.5 Hz and 5 Hz. To avoid phase shifts, all signals were filtered in forward and reverse directions with the MATLAB® function `filtfilt`.

Signal annotation: ECG R peak annotations were initialized with the Pan-Tompkins algorithm [6]. We used segments of 30 s to avoid high peaks, e.g. caused by motion artifacts, which distorted the thresholding in the Pan-Tompkins algorithm. Since many annotations were found to be a few samples off the R peak, an optimization process followed: For each annotation, the local gradient of the filtered ECG was calculated to both sides. The annotation was then shifted one sample towards the direction of the positive gradient. This process was repeated iteratively until the gradient to either side was less than or equal to zero, i.e. until the annotation reached the top of the R peak.

PPG onset annotations were derived with the function `qppg_fast` from the PhysioNet Cardiovascular Signal Toolbox 1.0.2 [7].

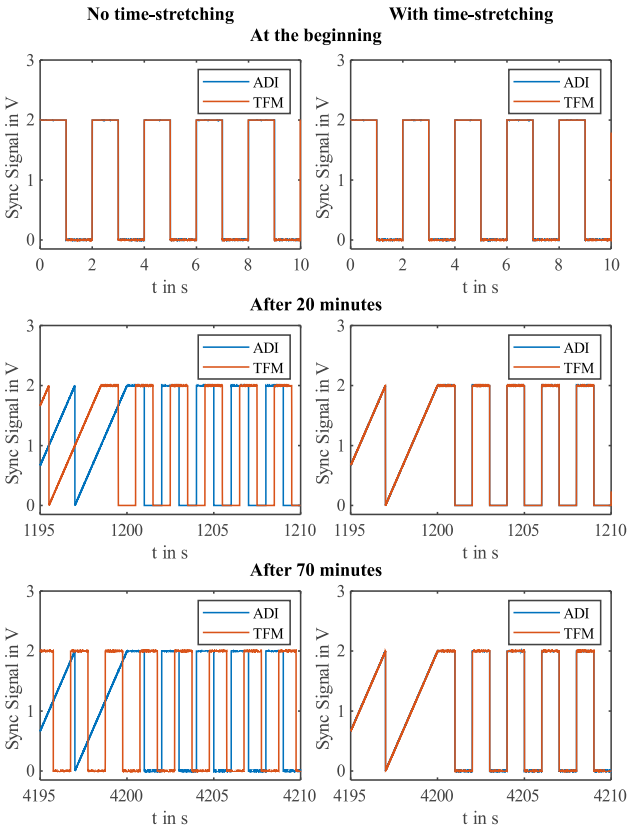

Figure 2: Sync signal of the ADInstruments PowerLab® (ADI) and the Task Force® Monitor (TFM) at different times. Left column: without time-stretching. Right column: with time-stretching. Time-stretching prevented the signals from diverging.

Annotation validation: Validation of the annotations was performed semi-automated. With 3 criteria, suspicious signal segments and annotations of the ECG were identified: (A) standard deviation of 2 s ECG segments larger than the standard deviation of the full ECG multiplied by a constant, (B) R peak amplitude smaller than a threshold, and (C) unusual changes in the tachogram (> ±20 % to preceding RR interval). The constant for (A) and the threshold for (B) were defined participant-specific in an interactive process with visual inspection of the resulting suspicious signal segments and annotations.

For the PPG signals, the criteria were limited to the unusual changes in the tachogram (> ±20 % to preceding

pulse-to-pulse interval) because signal distortions influence the onset detection in the PPG much stronger than this is the case with the R peak detection in the ECG, which means that distorted PPG signals led to suspicious tachogram segments.

The annotations within suspicious signal segments were then manually verified and, if necessary, corrected.

PAT calculation: Finally, PAT was calculated for each R peak annotation as the time difference between the R peak in the ECG and the ensuing pulse onset in the PPG (see Figure 3). Since this procedure does not require every R peak annotation to be followed by the corresponding pulse onset annotation, e.g. when pulse onset annotations from the finger PPG had to be removed due to movement artifacts, very long pulse arrival times not reflecting physiological information occurred. To avoid such outliers, the PAT values that differed more than three times the scaled median absolute deviation from the median were removed for each participant and PAT measure with the MATLAB® function `rmoutliers`.

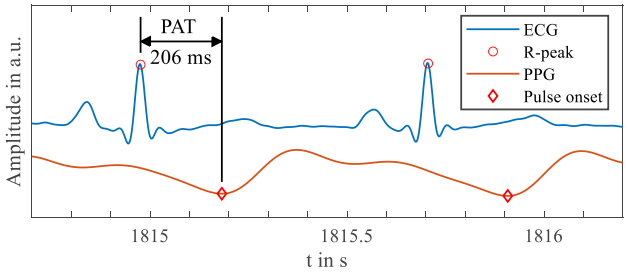

Figure 3: Definition of pulse arrival time (PAT). Electrocardiogram (ECG) channel Einthoven II and finger photoplethysmogram (PPG) were processed as described in section 2.2.

2.3 Evaluation

Finger PAT and earlobe PAT were evaluated identically. PAT was calculated for over 135,000 heart cycles from 42 healthy volunteers (20 female, 25.6 ± 5.1 years, BMI 22.0 ± 2.5 kg/m²). For each block and participant, a moving average filter with step size 10 was applied to the PAT series and the PAT mean of the block was calculated. To identify the effect of mental stress in our experiment, the PAT means of the blocks were statistically analyzed with the repeated measures ANOVA. Normality of all 12 distributions (2 PAT measures, 6 blocks) was tested with Shapiro-Wilk tests. All statistical analyses were performed with the software JASP 0.14.1 (University of Amsterdam, The Netherlands).

To gain a deeper insight, PAT from all heart cycles of all participants were visualized by state (rest vs. stress) in histograms with and without normalization to the mean value of the initial rest $\overline{\mathrm{PAT}}_{\mathrm{block1}}$. Other parameters provided by the TFM were investigated in a separate work [8].

3 Results

Figure 4 shows the finger and earlobe PAT distributions from all heart cycles of all participants across the two states with and without normalization. From all heart cycles, the earlobe PAT was 138 ± 21 ms at rest and 122 ± 22 ms under stress, and the finger PAT was 192 ± 17 ms at rest and 178 ± 20 ms under stress (mean ± standard deviation). This equals relative decreases of 11.6 % for the mean earlobe PAT and 7.3 % for the mean finger PAT under stress.

The Shapiro-Wilk tests confirmed that all 12 distributions were normally distributed. Repeated measures ANOVA showed significant differences between the block means for both PAT measures ($p < 0.001$, Greenhouse-Geisser correction) and returned large effect sizes ($partial\ \eta^2_{finger} = 0.45$, $partial\ \eta^2_{ear} = 0.56$). Post-hoc tests revealed significantly reduced PAT during the stress block compared to all five rest blocks for both PAT measures ($p < 0.001$, Bonferroni correction). We found no significant differences between the rest blocks in any combination. Figure 5 shows the mean finger and earlobe PAT across the blocks.

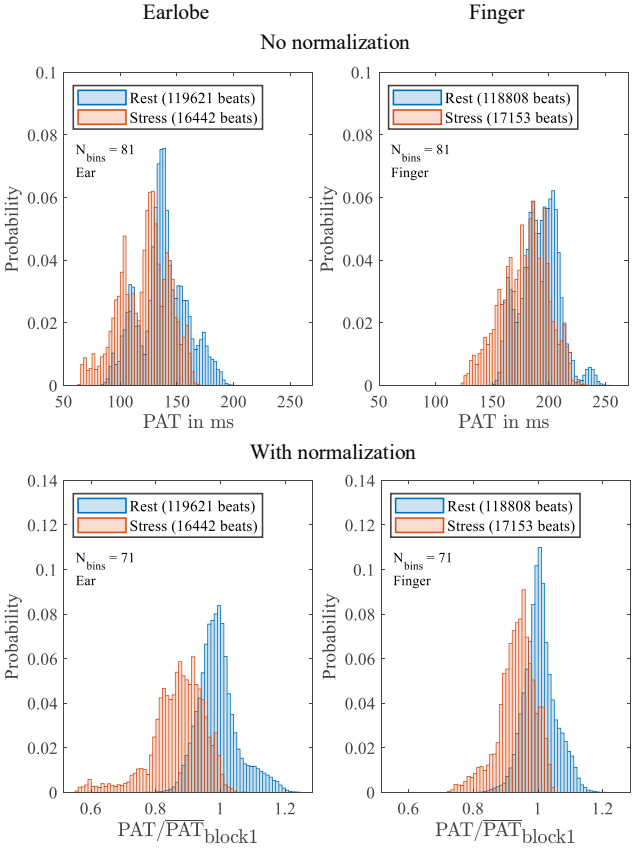

Figure 4: Distribution of all pulse arrival times (PAT) by state. Top row: no normalization. Bottom row: with normalization to the mean initial rest PAT of block 1. Left column: earlobe PAT. Right column: finger PAT.

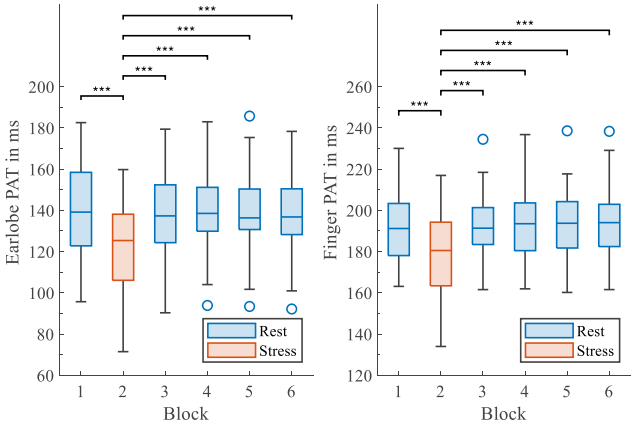

Figure 5: Results of the pulse arrival time (PAT) means for both measurement locations by block (42 participants). Left: earlobe PAT. Right: finger PAT. It should be noted that the scales of the ordinates differ. The pulse wave reaches the earlobe earlier than the finger and travels faster through the vascular system when stress is present. ***: $p < 0.001$.

The TFM measured mean blood pressure levels of 84 mmHg, 93 mmHg, 90 mmHg, 88 mmHg, 86 mmHg, and 85 mmHg for block 1 – 6 respectively, leading to an increase of 7.4 % under stress compared to average rest (86.6 mmHg).

4 Discussion

Our results affirm that the pulse wave reaches the earlobe faster than the index finger. This can be explained by a smaller distance between earlobe and heart, and in particular by the shorter peripheral vascular pathways [9]. In both measurement locations, PAT significantly decreased under stress indicating increased pulse wave velocity, which is attributed to elevated blood pressure [2], [3]. The absence of significant differences between the various rest blocks makes PAT a sensitive cardiovascular parameter for the detection of mental stress.

The synchronization procedure, the QRS detection, and the manual validation are conceivable limitations to the study. Synchronization presumed equidistant sampling as dynamic time warping algorithms were infeasible for such long signals. The annotation validation guaranteed complete control only in suspicious signal segments with unavoidable dependence on the inspector. However, PAT outlier removal and averaging decreased the influence of potentially incorrect annotations. The heuristic optimization of ECG annotations could presumably be spared with a more sophisticated QRS detector.

This study offers potential for several extensions. The inclusion of the impedance cardiogram would allow to estimate the pre-ejection period and infer pulse transit time instead of PAT. This has been found essential for the estimation of diastolic and mean blood pressure [2]. An alternative to contact PPG sensors are cameras [10]. Camera-based PPG provides spatio-temporal resolution and offers possibilities for novel analysis methods, e.g. the calculation of time offsets between multiple PPG signals acquired with a single sensor [11].

Author Statement

Research funding: This work was partly supported by grants of Deutsche Forschungsgemeinschaft (German Research Foundation DFG 319919706/GRK2323) and the European Regional Development Fund (ERDF 100278533). Conflict of interest: Authors state no conflict of interest. Informed consent: Informed consent has been obtained from all individuals included in this study. Ethical approval: The research related to human use complies with all the relevant national regulations, institutional policies and was performed in accordance with the tenets of the Helsinki Declaration, and has been approved by the authors' institutional review board.

References

[1] Klabunde RE. Cardiovascular Physiology Concepts. 2nd ed. Philadelphia: Lippincott Williams & Wilkins, 2011.
[2] Buxi D, Redouté JM, Yuce MR. A survey on signals and systems in ambulatory blood pressure monitoring using pulse transit time. Physiol Meas 2015;36:R1–R26.
[3] Steptoe A, Smulyan H, Gribbin B. Pulse Wave Velocity and Blood Pressure Change: Calibration and Applications. Psychophysiology 1976;13:488–493.
[4] Kolotylova T, Koschke M, Bär KJ, Ebner-Priemer U, Kleindienst N, Bohus M, Schmahl C. Entwicklung des „Mannheimer Multikomponenten-Stress-Test" (MMST). Psychother · Psychosom · Med Psychol 2010;60:64–72.
[5] Reinhardt T, Schmahl C, Wüst S, Bohus M. Salivary cortisol, heart rate, electrodermal activity and subjective stress responses to the Mannheim Multicomponent Stress Test (MMST). Psychiatry Res 2012;198:106–111.
[6] Pan J, Tompkins WJ. A Real-Time QRS Detection Algorithm. IEEE Trans Biomed Eng 1985;BME-32:230–236.
[7] Vest AN, Da Poian G, Li Q, Liu C, Nemati S, Shah AJ, Clifford GD. An Open Source Benchmarked Toolbox for Cardiovascular Waveform and Interval Analysis. Physiol Meas 2018;39:105004.
[8] Ernst H, Pannasch S, Helmert JR, Malberg H, Schmidt M. Cardiovascular Effects of Mental Stress in Healthy Volunteers. In: 48th Conf Computing in Cardiology (CinC). Brno: IEEE; 2021;(in press).
[9] Tillmann BN. Atlas der Anatomie des Menschen. 3rd ed. Berlin, Heidelberg: Springer; 2016:92,444–455.
[10] Kamshilin AA, Sidorov IS, Babayan L, Volynsky MA, Giniatullin R, Mamontov OV. Accurate measurement of the pulse wave delay with imaging photoplethysmography. Biomed Opt Express 2016;7:5138.
[11] Zaunseder S, Trumpp A, Ernst H, Förster M, Malberg H. Spatio-temporal analysis of blood perfusion by imaging photoplethysmography. In: Coté GL, editor. Optical Diagnostics and Sensing XVIII: Toward Point-of-Care Diagnostics. San Francisco: SPIE; 2018:178–191.